Particle multiplicities and ratios in excluded volume models

M. Mishra* and C. P. Singh†
Department of Physics, Banaras Hindu University, Varanasi 221 005, India
(Received 17 March 2008; revised manuscript received 28 June 2008; published 28 August 2008)

One of the most surprising results is to find that a consistent description of all the experimental results on particle multiplicities and ratios obtained from the lowest Alternating Gradient Synchrotron to the highest Relativistic Heavy Ion Collider energies is possible within the framework of a thermal statistical model. We explore here the utility of a thermodynamically consistent excluded volume model recently proposed by us in explaining the above experimental results and we further compare our results with those obtained from an ideal gas model and other excluded-volume model that are often used in describing a grand canonical statistical system consisting of hot, dense hadron gas. We find that the energy dependence of the total multiplicities of strange and nonstrange hadrons in general shows close agreement with the experimental data, although slight deviation is observed for some multistrange hadrons, e.g., $\Omega + \bar{\Omega}$, Ξ, and Φ. The difference observed in these cases does not clearly support our assumption of the same freeze-out volume of the fireball that homogeneously emit all kinds of particles. Similarly we have calculated the ratios for particles and antiparticles such as K^-/K^+, $\bar{p}/p$, $\bar{\Lambda}/\Lambda$, $\bar{\Xi}/\Xi$, and $\bar{\Omega}/\Omega$, as well as the ratios of the unequal mass particles $\langle K^+\rangle/\langle\pi^+\rangle$, $\langle K^-\rangle/\langle\pi^-\rangle$, $\langle\Lambda\rangle/\langle\pi\rangle$, $\langle\Xi^-\rangle/\langle\pi\rangle$, $\langle\Omega+\bar{\Omega}\rangle/\langle\pi\rangle$, and $\langle\Phi\rangle/\langle\pi\rangle$ and studied their variations with respect to the center-of-mass energy in the excluded-volume models and, finally, the results are compared with the experimental data. We find that in some cases, although the calculated results show close agreements with the experimental data, the deviations between theory and experiment in cases of unequal mass and multistrange particle ratios, like $\langle\Lambda\rangle/\langle\pi\rangle$, $\langle\Xi^-\rangle/\langle\pi\rangle$, $\langle\Omega+\bar{\Omega}\rangle/\langle\pi\rangle$, $\langle\Phi\rangle/\langle\pi\rangle$, etc., appear to be quite large and thus warrant further investigations on the suitability of thermal hadron gas models.

DOI: 10.1103/PhysRevC.78.024910 PACS number(s): 25.75.Nq, 24.10.Pa

I. INTRODUCTION

In ultrarelativistic heavy-ion collisions, we expect that matter with high energy density will be produced and color-deconfined matter is formed. Such matter, better known as quark-gluon plasma (QGP), is only a transient state of the system because evolution back to ordinary hadronic matter begins immediately [1–3]. Consequently, we face a difficult question regarding how to diagnose and probe the plasma state. One of the most potential probes for detecting QGP formation is the observation of the abundance of strange particles. The idea behind the strangeness enhancement is that strange and antistrange quarks are easily created in a hot and dense QGP, whereas in the hadronic phase, $K\bar{K}$ pair production is suppressed. One finds that the threshold mass for $s\bar{s}$ production is nearly 300 MeV/c^2 in QGP, whereas the $K\bar{K}$ threshold mass is approximately 980 MeV/c^2. Rafelski and Müller [4–10] have suggested that a large number of strange quarks present in QGP would automatically yield enhanced strange particle production in the hadron gas (HG) resulting after hadronization of QGP. However, one important assumption in the theory is that the HG formed after QGP phase does not find sufficient time to achieve chemical equilibrium, otherwise the equilibrated HG will not retain the memory regarding the primordial phase that might have existed earlier in the evolution process. However, in the analysis of strangeness enhancement, one should have a precise knowledge not only of the equation of state (EOS) of QGP alone but also of the HG that gives the background contribution in this case.

In ultrarelativistic nucleus-nucleus collisions, a very high density of matter exists over an extended region, and it is often called a *fireball*. The physical variables characterizing a fireball are the energy density ϵ, the baryon density n_B, and the volume. Thus one of the central problems in the study of high-energy collisions lies in deducing the state of the system by determining the temperature and baryon chemical potential μ_B (which in turn determine ϵ and n_B) existing in the fireball from the observed final particle multiplicities, etc. The freeze-out stage of the system when the particles fly toward the detectors without further interactions is directly connected to the observed multiplicity distributions of various particles. Here we should emphasize that the fireball goes through two types of freeze-out stages. First, it undergoes a chemical freeze-out when inelastic collisions in the fireball no longer occur. Later when elastic collisions also stop in the fireball, the stage is called thermal freeze-out. Abundances of the particles and their ratios provide important information regarding the chemical equilibrium occurring in the fireball before the thermal equilibrium. Moreover, chemical equilibrium in the hot, dense HG removes any memory existing in the fireball regarding a primordial phase transition. So the thermodynamic properties of the fireball throw no light on the existence of QGP before hadronization. We first connect the thermodynamic properties of the fireball to an appropriate EOS for the hot and dense hadron gas and, finally, we deduce the chemical freeze-out conditions of the thermal HG fireball formed in the ultrarelativistic heavy-ion collisions. In the last few years, one has observed a very surprising result. It has been shown that a consistent and appropriate description of all the experimental

*madhukar.12@gmail.com
†cpsingh_bhu@yahoo.co.in

results on the particle multiplicities and particle ratios from the lowest GSI Schwerionen Synchrotron (SIS) to the highest Relativistic Heavy Ion Collider (RHIC) energies is available within the framework of a thermal statistical model as applied to a hot and dense HG phase. Recently we provided a model based on the geometrical excluded volume correction that describes suitably the thermodynamical quantities of a hot and dense HG [11]. We further used this prescription to determine the chemical freeze-out volume of the fireball and thus we calculated pion and nucleon densities in our model [12]. We find that the densities are reproduced well by their Hanbury-Brown-Twiss experimental data.

In this article we attempt to explain the experimental data on strange particle multiplicities and ratios in the HG scenario using our excluded volume model discussed in earlier articles [11,12]. Because many attempts [13] have been made by various authors to explain particle multiplicities using different HG models [14–18], it will be worthwhile to compare chemical freeze-out parameters (i.e., T, μ_B) of the fireball as determined in these models. Finally, we show our results for strange particle multiplicities and ratios and compare them with the experimental data. We also show the predictions of the other important models, particularly the Rischke, Gorenstein, Stöcker, and Greiner (RGSG) [19] model that is, again, a thermodynamically consistent excluded volume model [19]. It is indeed encouraging to notice that simple thermal models can explain well the experimental data on particle multiplicities and the strangeness enhancement. But the purpose here is to demonstrate that the whole exercise crucially depends on the EOS used to determine the thermodynamic state of the fireball of the hot and dense HG.

II. METHOD OF CALCULATION

We have formulated a new thermodynamically consistent excluded-volume model [11] for the description of hot and dense HG. By incorporating the finite size of the baryons, here we obtain a simple form of EOS for the HG where the excluded volume effect has been incorporated in the partition function by suitably defining the volume integral. Our approach has many advantages over other models existing in the literature [19,20] as it can suitably be used even at extreme values of T and μ_B. We also find that causality is respected by our model. Further, the final expressions in our model are quite similar to those of the Cleymans and Suhonen model [21], which is a thermodynamically inconsistent description of the HG. However, our model involves extra terms in the final expressions as the correction terms arising from the requirement of thermodynamical consistency. In the following, we present a brief description of our model for the sake of completeness. This model assumes that the baryon of ith species have an eigenvolume V_i. If $R = \sum_i n_i^{\rm ex} V_i$ be the fraction of occupied volume, then the number density $n_i^{\rm ex}$ of ith baryon can be written as:

$$n_i^{\rm ex} = (1 - R)\, I_i\, \lambda_i - I_i\, \lambda_i^2\, \frac{\partial R}{\partial \lambda_i}, \tag{1}$$

where λ_i is the fugacity of ith baryons and I_i is the following expression containing the modified Bessel function of the second kind

$$I_i = \frac{g_i}{2\pi^2} \left(\frac{m_i}{T}\right)^2 T^3\, K_2(m_i/T) \tag{2}$$

with g_i is the spin-isospin degeneracy factor. Equation (1) can be rewritten in the form

$$R = (1 - R) \sum_i n_i^0\, V_i - \sum_i n_i^0\, V_i\, \lambda_i\, \frac{\partial R}{\partial \lambda_i}, \tag{3}$$

where n_i^0 is the number density of ith baryons when they are treated as pointlike particles and thus $n_i^0 \equiv I_i\, \lambda_i$. Let us take $R^0 \equiv \sum_i X_i$, where $X_i \equiv I_i\, \lambda_i\, V_i$. If we put $\partial R/\partial \lambda_i = 0$, then

$$R \equiv \hat{R} = \frac{R^0}{1 + R^0}. \tag{4}$$

Equation (4) gives the thermodynamic inconsistent expression for R in the model of Cleymans and Suhonen [21], the number density $n_i^{\rm ex}$ of ith baryon is given as $n_i^{\rm ex} = n_i^0/(1 + R^0)$ that resembles Eq. (4). Hence the additional term $\partial R/\partial \lambda_i$ in Eq. (3) restores thermodynamic consistency in our model. Rewriting Eq. (3), we get:

$$R = \hat{R} + \Omega R, \tag{5}$$

where the operator Ω is given as

$$\Omega \equiv -\frac{1}{1 + R^0} \sum_i I_i\, \lambda_i^2\, V_i\, \frac{\partial}{\partial \lambda_i}. \tag{6}$$

Now using Neumann iteration method, Eq. (3) can be cast in the form

$$R = \hat{R} + \Omega \hat{R} + \Omega^2 \hat{R} + \Omega^3 \hat{R} + \cdots. \tag{7}$$

Retaining the terms up to second order only, the expression for R can be written as

$$R = \frac{\sum_i X_i}{1 + \sum X_i} - \frac{\sum_i X_i^2}{\left(1 + \sum_i X_i\right)^3} + 2\frac{\sum_i X_i^3}{\left(1 + \sum_i X_i\right)^4} - 3\frac{\sum_i X_i\, \lambda_i \sum_i X_i^2\, I_i\, V_i}{\left(1 + \sum_i X_i\right)^5}. \tag{8}$$

Finally, by calculating the values of R and its first derivative $\partial R/\partial \lambda_i$, one can calculate the value of particle number density by using Eq. (1).

We have considered here a hot and dense HG with baryonic and mesonic resonances having masses up to 2 GeV/c^2. To conserve strangeness quantum number, we used the criterion of net strangeness number density equal to zero. In all the above calculations we also considered that all the mesons behave as pointlike particles. Furthermore, we took equal volume $V = 4\pi\, r^3/3$ for all baryons with a hard-core radius $r = 0.8$ fm. Here it should be emphasized that the finite width of the resonances are not taken into account in the present calculation. The grand canonical ensemble approach as used here is suitable for systems with large number of produced hadrons. For small systems and for low energies, in the case of strange particle production, a canonical ensemble treatment is necessary [22]. It leads to a phase-space reduction for particle production (known as canonical suppression). It has been shown [23] that the canonical suppression factor is

negligible for all strange hadrons above Alternating Gradient Synchrotron (AGS) energies ($\sqrt{s_{NN}} \approx 5$ GeV) but it yields a sizable correction for the lower energies. We have not incorporated the canonical correction in the present analysis because our results are mostly valid for energies above AGS energies.

We consider all hadronic resonances having well-defined masses, i.e., their decay widths are small. All hadronic resonances decay rapidly in strong decays after freeze-out and thus contribute to the stable particle abundances. Some heavy resonances may decay in cascades. This has been implemented in the calculation by considering all decays proceeding sequentially from the heaviest to lightest particles. As a consequence of this, the light particles get contributions from the heaviest particles. Thus it has the form:

$$n_1 = b_{2\to 1} \cdots b_N \, b_{N-1} \, n_N,$$

where $b_{k\to k-1}$ combines the branching ratios for the $k \to k-1$ decay [24] with the appropriate Clebsch-Gordan coefficients. The later accounts for the isospin symmetry in strong decays and allows us to treat separately the different charged states of isospin multiplets of particles. To calculate contributions from some heavy resonance decays we are forced to take some approximations. For example, in most of the cases there are several decay channels. In our approach we discard all decays with branching ratios less than 2%. In addition, if the decay channels are classified as dominant, largely seen, or possibly seen, we take into account the dominant channel only. If two or more than two channels are described as equally important, we take all of them with the same weight. For example, $f_0(980)$ decays into π (according to Ref. [24] this is the dominant channel) and $K\bar{K}$ (according to Ref. [25] this is the seen channel). In our approach, as a rule stated above, we include only the process $f_0(980) \to \pi$. Similarly, $a_0(1450)$ has three decay channels: $\eta\pi$ (seen), $\pi\eta'$ (958) (seen), and $K\bar{K}$ (again seen). In this case we include all the three decay channels with equal weight 0.33 (branching ratios). Of course, this procedure is not unique and may vary from author to author. Another problem that we face in this calculation is that in some decay channels, the branching ratios are not given exactly but a range of values are given and the sum of the branching ratios may differ significantly from 1.0. In this case we take the mean values of the branching ratios. Because we require that their sum should be properly normalized, we are forced to rescale all the mean values in such a way that their sum is indeed 1.0. Because the experimental data on the resonances involve a lot of uncertainties in the decay width as well as in the branching ratios, we adopt the above procedure in calculating the contributions of resonances toward a given particle multiplicity. Unfortunately, a better and established alternative for such calculation does not exist in the literature.

TABLE I. List of particle ratios used to fit different models [13].

$\sqrt{s}$ (GeV)	Experiments	Particle ratios
2.70	AGS	K^+/π^+
		p/π^-
		Λ/π^-
3.32, 3.84, 4.30	AGS	K^-/K^+
		K^+/π^+
		K^-/π^-
		p/π^-
		Λ/π^-
4.85	AGS	K^-/K^+
		K^+/π^+
		K^-/π^-
		p/π^-
		Λ/π^-
		$\bar{p}/p$
		$\bar{\Lambda}/\Lambda$
8.76	SPS	K^-/K^+
		$\bar{\Lambda}/\Lambda$
		K^+/π^+
		K^-/π^-
		$\bar{\Lambda}/\pi^-$
		Ξ/π^-
		Ξ/Λ
		Ω/Ξ
12.3	SPS	K^-/K^+
		$\bar{\Lambda}/\Lambda$
		K^+/π^+
		K^-/π^-
		$\bar{\Lambda}/\pi^-$
17.3	SPS	K^-/K^+
		$\bar{\Lambda}/\Lambda$
		$\bar{\Xi}/\Xi$
		$\bar{\Omega}/\Omega$
		K^+/π^+
		K^-/π^-
		$\bar{\Lambda}/\pi^-$
		Ξ/π^-
		Ω/π^-
130, 200	RHIC	K^-/K^+
		$\bar{\Lambda}/\Lambda$
		$\bar{\Xi}/\Xi$
		$\bar{\Omega}/\Omega$
		K^+/π^+
		K^-/π^-
		$\bar{p}/p$
		p^-/π^-
		$\bar{\Lambda}/\pi^-$
		Ξ/π^-
		Ω/π^-

III. RESULTS AND DISCUSSIONS

To determine the energy dependence of particle ratios and multiplicities we first find energy dependence of chemical freeze-out temperature and baryon chemical potential by fitting the different particle ratios from SIS to RHIC energies using ideal HG model, RGSG model as well as present model. In Table I, we have given the list of particle ratios [13] that had been used to calculate T, μ_B values at freeze-out for different energies. Table II summarizes the values of T and μ_B at different center-of-mass energies in different models. We find that T and μ_B obtained in our model can be parameterized in terms of center-of-mass energy by using following

TABLE II. $(T,\ \mu_B)$ values in MeV obtained by fitting the particle ratios using different models.

$\sqrt{s_{NN}}$ (GeV)	Ideal gas model			RGSG model			Present model		
	T	μ_B	δ^2	T	μ_B	δ^2	T	μ_B	δ^2
2.70	60.0	740.0	0.85	60.0	740.0	0.75	60.0	740.0	0.87
3.32	80.0	670.0	0.89	78.0	680.0	0.34	90.0	670.0	0.69
3.84	100.0	645.0	0.50	86.0	640.0	0.90	100.0	650.0	0.60
4.30	101.0	590.0	0.70	100.0	590.0	0.98	101.0	600.0	0.53
4.85	105.0	495.0	0.30	130.0	535.0	0.84	110.0	510.0	0.43
8.76	140.0	380.0	0.45	145.0	406.0	0.62	140.0	380.0	0.26
12.3	148.0	300.0	0.31	150.0	298.0	0.71	148.6	300.0	0.31
17.3	160.0	255.0	0.25	160.0	240.0	0.62	160.6	250.6	0.21
130.0	172.3	35.53	0.10	165.5	38.0	0.54	172.3	28.0	0.056
200.0	172.3	23.53	0.065	165.5	25.0	0.60	172.3	20.0	0.043

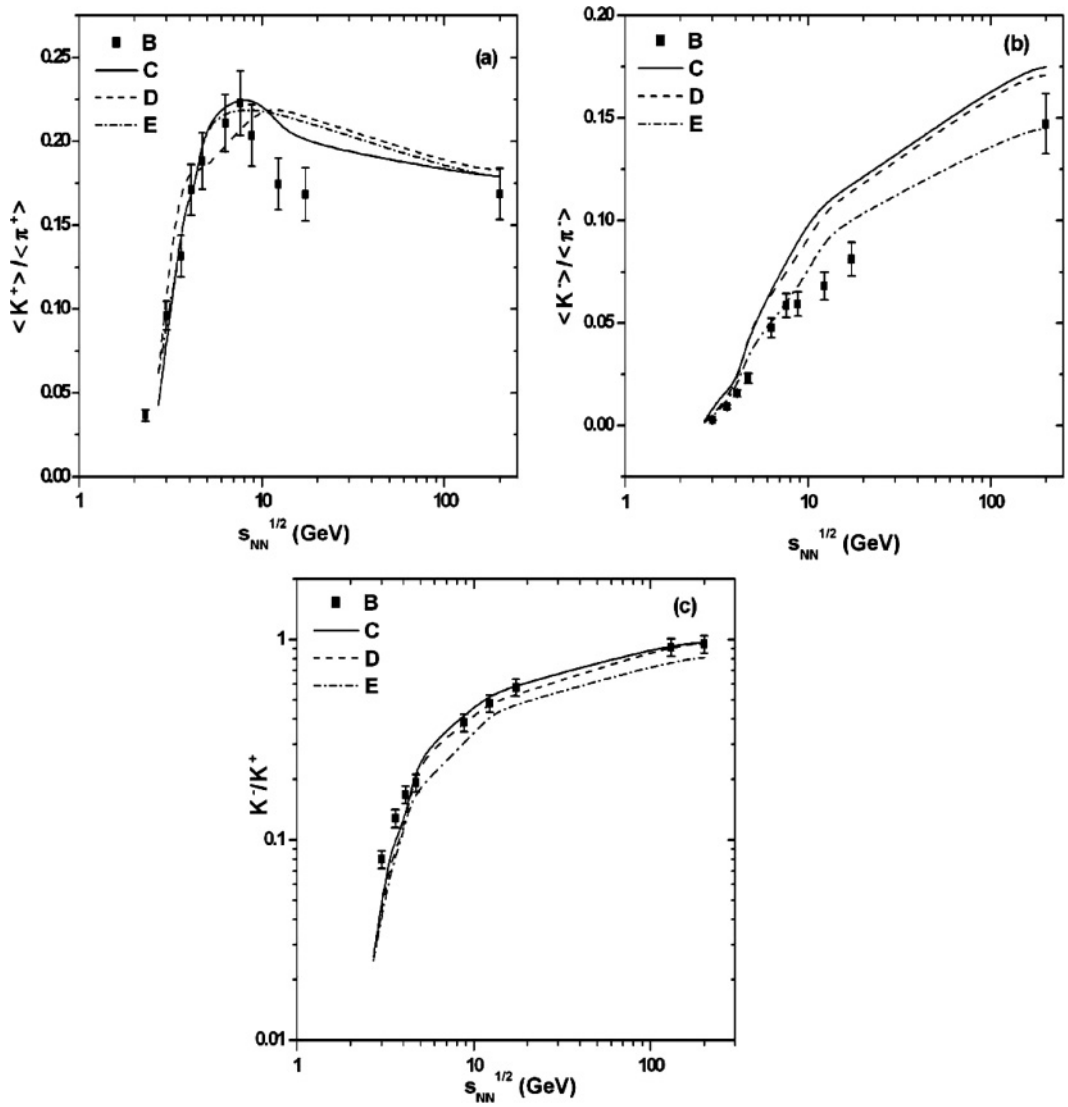

FIG. 1. (a), (b), and (c) Variations of the strange meson to nonstrange meson ratios $\langle K^+\rangle/\langle\pi^+\rangle$, $\langle K^-\rangle/\langle\pi^-\rangle$ and antikaon-to-kaon ratio K^-/K^+ with respect to center-of-mass energy $\sqrt{s_{NN}}$. Solid curve (C), dashed curve (D), and dash-dotted curve (E) show the predictions of the present [11,12], ideal HG, and RGSG models [19], respectively. B represents experimental points [32].

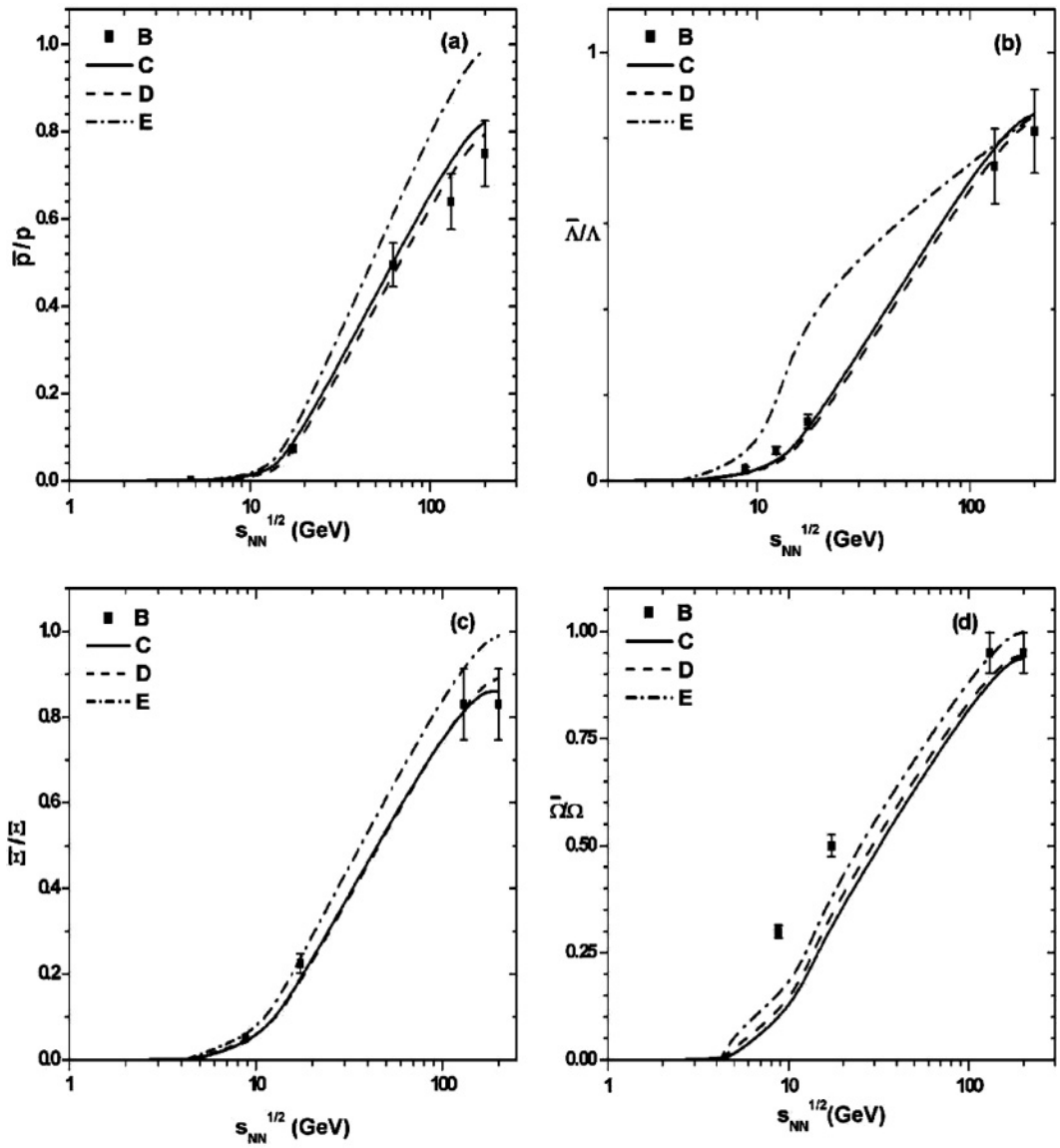

FIG. 2. (a), (b), (c), and (d) Variations of the antibaryon-to-baryon ratios $\bar{p}/p$, $\bar{\Lambda}/\Lambda$, $\bar{\Xi}/\Xi$, and $\bar{\Omega}/\Omega$ with respect to center-of-mass energy. B represents experimental data, whereas curves C, D, and E show the results from the present model, ideal HG model, and RGSG model, respectively.

equations [26–29]:

$$\mu_B = \frac{a}{1 + b\sqrt{s_{NN}}}, \qquad T = c - d\, e^{-f\sqrt{s_{NN}}}. \tag{9}$$

Here the values of the parameters as arising from the best fit are $a = 1.254 \pm 0.086$ GeV, $b = 0.261 \pm 0.034$ GeV^{-1} and $c = 168.49 \pm 4.4$ MeV, $d = 171.63 \pm 21.75$ MeV, $f = 0.21 \pm 0.039$ GeV. We compare our values of the above parameters with the values of the parameters $a = 1.308 \pm 0.028$ GeV, $b = 0.273 \pm 0.008$ GeV^{-1} and $c = 172.3 \pm 2.8$ MeV, $d = 149.5 \pm 5.7$ MeV, $f = 0.20 \pm 0.03$ GeV obtained by Cleymans *et al*., in ideal HG prescription [28,29]. We find that the difference in the values of the parameters as obtained by us as well as other authors does not appear to differ very significantly. Recently it has become abundantly clear that the heavy-ion collision energy plays an important role in determining the properties of the final-state hadrons. We find that the extracted temperature generally increases rapidly, whereas baryon chemical potential monotonically decreases with the collision energy. In general, extracted freeze-out values of these parameters in our model lie close to the ideal gas values. The parameter values in RGSG model are, however, found to differ in comparison to our values. Particle multiplicities and ratios can then be calculated using T and μ_B values presented in Table II.

In Figs. 1(a)–1(c), we show the center-of-mass energy dependence of the ratio of strange meson to nonstrange meson such as $\langle K^+\rangle/\langle\pi^+\rangle$, $\langle K^-\rangle/\langle\pi^-\rangle$, and K^-/K^+ in our present model [11,12], in an ideal HG model, and in the RGSG model [19]. Solid, dashed, and dash-dotted curves represent

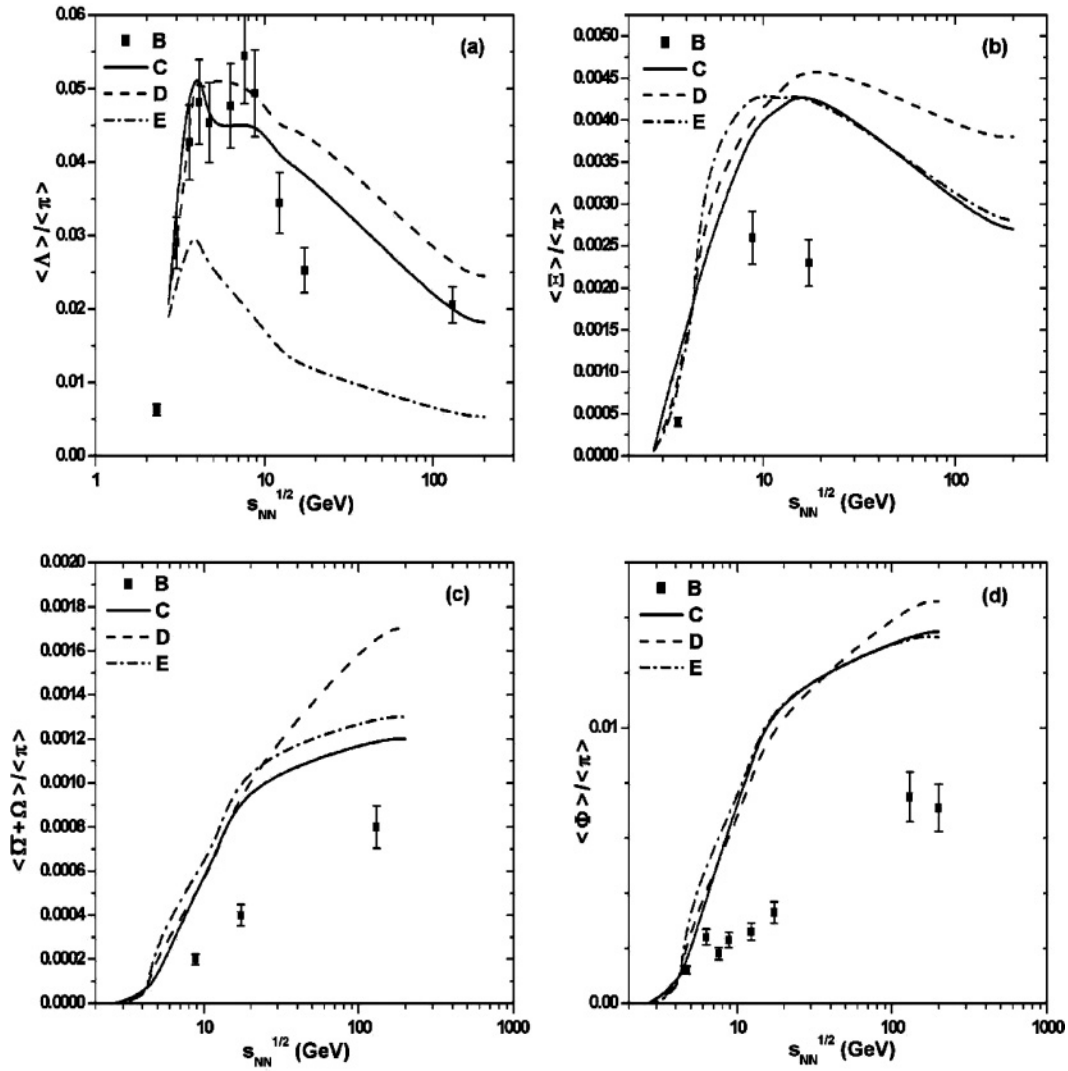

FIG. 3. (a), (b), (c), and (d) Variations of the strange baryon to nonstrange meson ratios $\langle\Lambda\rangle/\langle\pi\rangle$, $\langle\Xi\rangle/\langle\pi\rangle$ and $\langle\Omega+\bar{\Omega}\rangle/\langle\pi\rangle$, $\langle\Phi\rangle/\langle\pi\rangle$ with the center-of-mass energy $\sqrt{S_{NN}}$. In this figure curves B represents experimental data [33] and curves C, D, and E depict the predictions of the present model, ideal HG model, and RGSG model, respectively.

predictions of our model, the ideal HG model, and the RGSG model, respectively. The $\langle K^+\rangle/\langle\pi^+\rangle$ ratio shows a peak at around 8.0 GeV of center-of-mass energy, although the ratio $\langle K^-\rangle/\langle\pi^-\rangle$ shows a monotonic increase with center-of-mass energy $\sqrt{s_{NN}}$ and achieves a saturation at or around the RHIC energy. Essentially the saturation arises as the freeze-out temperatures that become almost constant at or around RHIC energies. The peak in the $\langle K^+\rangle/\langle\pi^+\rangle$ ratio is demonstrated in all the thermal models [30,31] and this successful explanation of the experimental data is one important feature of the thermal models. However, the peak in these models is slightly broader than that observed by the experiments. Our thermal model shows a narrow peak at the same energy as given by the experimental data. However, our theoretical points differ from the experimental points at higher energies [32]. Other types of models, like the transport model, etc., are not able to explain the experimental features of the $\langle K^+\rangle/\langle\pi^+\rangle$ ratio. However, all types of thermal models provide a larger ratio for $\langle K^-\rangle/\langle\pi^-\rangle$ than that observed in the experiments. Still, the main features of the data showing a steady increase is also reproduced by all thermal models. The ratio K^-/K^+ and its variation with center-of-mass energy is shown in Fig. 1(c). The ratio K^-/K^+ shows much dependence on the center-of-mass energy. Our thermal model prediction for the ratio K^-/K^+ shows a close agreement with the predictions of other models. The feature of the experimental curve is also in good agreement with our thermal model calculation.

In Figs. 2(a)–2(d), we plot the energy dependence of the antibaryon-to-baryon ratios like $\bar{p}/p$, $\bar{\Lambda}/\Lambda$, $\bar{\Xi}/\Xi$, and $\bar{\Omega}/\Omega$ as given by our present model, the ideal HG model, and the RGSG model. Surprisingly, we find that our present model and the ideal HG model reproduce the qualitative and quantitative features of the experimental data for all these ratios. This occurs because the freeze-out values of T and μ_B at different energies do not differ much in these two models. However, the predictions in the calculations of RGSG model do not show

such agreement with the experimental data. As we pointed out earlier [11], the ideal HG description does not provide a proper EOS for hot and dense HG. The successful explanation of the experimental results shows that a proper and realistic EOS for HG is given by our model that also gives a thermodynamically consistent description of the hot and dense HG.

Figures 3(a)–3(d) show the variation of the particle ratios like $\langle\Lambda\rangle/\langle\pi\rangle$, $\langle\Xi\rangle/\langle\pi\rangle$, and $\langle\Omega+\bar{\Omega}\rangle/\langle\pi\rangle$, $\langle\Phi\rangle/\langle\pi\rangle$ with the center-of-mass energy $\sqrt{s_{NN}}$ in all the above three models. We find that results in our present calculation, particularly of $\langle\Lambda\rangle/\langle\pi\rangle$, show agreement with the experimental data [33] because our curve reproduces the main features of the data. The ideal hadron gas model also gives a satisfactory explanation but calculated results lie numerically above the experimental points. The main problem comes when we compare predictions from all these models for multistrange particle ratios, e.g., $\langle\Xi\rangle/\langle\pi\rangle$, $\langle\Omega+\bar{\Omega}\rangle/\langle\pi\rangle$, and $\langle\Phi\rangle/\langle\pi\rangle$ as shown by Figs. 3(b)–3(d). We find that in all these cases, thermal models involving HG picture alone yield a large difference with the experimental data and in fact theoretical curves lie far above the curves given by the experimental data. Here, Ξ is ssu (or ssd), Ω is sss, and Φ is given by $s\bar{s}$ quark combinations. These results not only signify the failure of all types of thermal models but also emphasize the need for going beyond such approaches for the cases of multistrange hadrons. The strangeness enhancement signals QGP formation but in these cases, thermal models yield much larger strangeness than that observed in the experiments. Usually one uses a new parameter γ_s to get a fit to the whole data points. γ_s is called the strangeness saturation factor and its value lies in the range $0 < \gamma_s < 1$. It allows us to parametrize the incomplete chemical equilibration of the strange particles so all the ratios can be fitted simultaneously with the same values of μ_B and T. We define the effective fugacity of each strange quark as $\gamma_s\,\lambda_s$ and that of strange antiquark as $\gamma_s\,\lambda_s^{-1}$. Obviously ratios like $\bar{\Lambda}/\Lambda$ and $\bar{\Xi}/\Xi$ will not be affected but ratios like Λ/π or Φ/π, etc., will be smaller because γ_s in HG is usually less than 1 but close to 1. In the calculation $\lambda_q = \exp(\mu_q/T)$ and $\lambda_s = \exp(\mu_s/T)$, where $\mu_B = 3\mu_q$ and $\mu_s = -\mu_S + \mu_B/3$. It was found that experimental data at the CERN Super Proton Synchrotron can be easily explained with the help of γ_s. However, saturation of strangeness phase space should occur within the time scale of Pb+Pb or Au+Au collisions and therefore the need for additional parameters should not arise in our calculation. So we still feel that ratios like $\langle\Lambda\rangle/\langle\pi\rangle$, etc., can be explained if some modification of the model is done properly. We want to emphasize that several authors have used a quark coalescence model in the QGP picture [34–39] to explain these anomalous results.

Here one must emphasize that we have used the freeze-out volume obtained for K^+ meson to deduce total particle multiplicity for each type of hadron. We use experimental data of multiplicity for K^+ and divide it by the number density of K^+ that was obtained in our thermal model. This yields the chemical freeze-out volume for K^+ when emissions from the fireball occurs. We have assumed that the fireball goes through the stage of chemical equilibrium among its various constituents and the freeze-out volume of the fireball for the emissions of all types of hadrons remains the same. To test the validity of this assumption, we have plotted the total freeze-out volume for π^+, K^+, K^-, respectively, in Fig. 4 and study its variation with center-of-mass energy. We find that the freeze-out volumes obtained for these particles do not overlap and a constant difference in the curves exist at all energies. This is again a significant result as it can also be used to explain the experimental data of the ratio of unequal mass particles. In our earlier article, we have demonstrated [12] how we can use the freeze-out volume to explain the occurrence of a first-order phase transition.

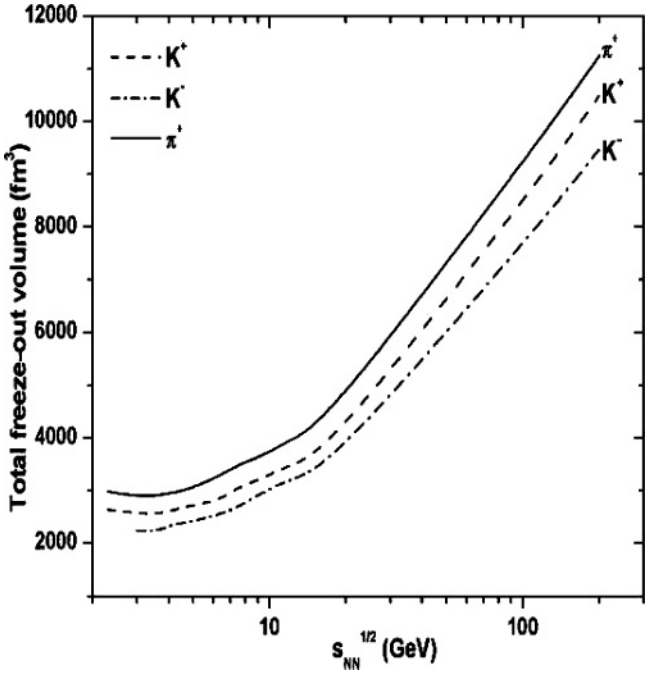

FIG. 4. Variations of total freeze-out volume V of K^-, K^+, and π^+ with respect to $\sqrt{s_{NN}}$.

In Fig. 5, we show the center-of-mass energy dependence of multiplicities of hadrons $\bar{\Lambda}$, $(\Omega+\bar{\Omega})$, Ξ^-, Λ, Φ, K^-, K^+, and π^+ as predicted by calculations in our present model. Curves A, B, C, and D show the multiplicities of $\bar{\Lambda}$, $\Omega+\bar{\Omega}$, Ξ^-, and Λ baryons scaled by factors of 0.02, 0.2, 0.1, and 0.02, respectively. Curves E, F, G, and H depict the multiplicities of Φ, K^-, K^+, and π^+ mesons, respectively. We have also shown here experimental results measured in central Au+Au/Pb+Pb collisions [40–56] for comparison. Here we extracted the freeze-out volume of the fireball from the calculated number density of K^+ and compared it with total multiplicity of K^+ experimental data. We use the same volume for all other particles. We observe an excellent agreement between the theoretical predictions by our present thermal model and the experimental data for the total multiplicities of π^+, K^+, K^-, Λ, $\bar{\Lambda}$, etc. However, the thermal model calculation slightly differs for $\Omega+\bar{\Omega}$, Ξ, and Φ as compared to experimentally measured values. Thermal values of the multiplicities for all these particles are again larger than the experimental values. This analysis again suggests a new and different mechanism for the production of these particles. One way out of this difficulty is to assume that these particles achieve chemical equilibrium earlier in the fireball when the

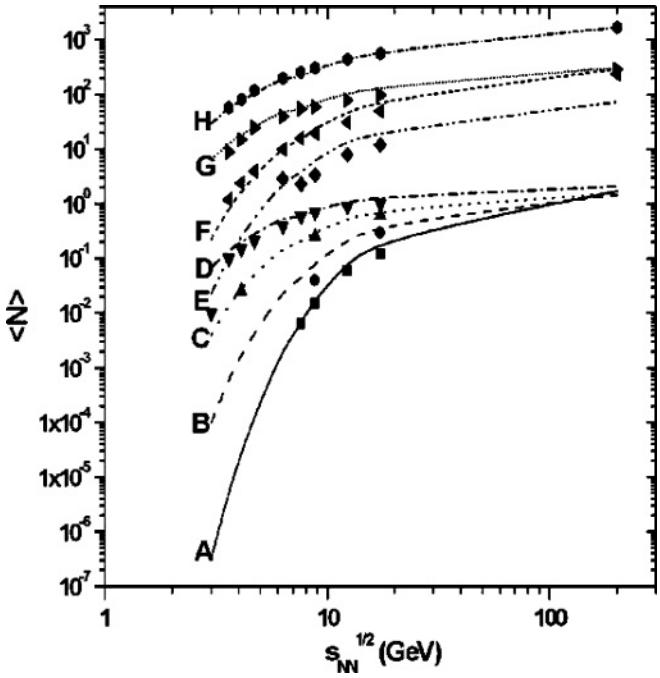

FIG. 5. Variations of total multiplicities of $\bar{\Lambda}$, $(\Omega + \bar{\Omega})$, Ξ^-, Λ, Φ, K^-, K^+, and π^+ with respect to center-of-mass energy predicted by our present model. Experimental data measured in central Au+Au/Pb+Pb collisions [40–56] have also been shown for comparison. In this figure A represents multiplicity of $\bar{\Lambda}$ (scaled by a factor 0.02), B that of $\Omega + \bar{\Omega}$ (scaled by 0.2), C that of Ξ^- (scaled by 0.1), and D that of Λ (scaled by 0.02). Similarly, E, F, G, and H represent the multiplicities of Φ, K^-, K^+, and π^+ mesons, respectively.

corresponding volume is much smaller. However, this is a vexing problem that appears in the use of thermal models and we have to find appropriate answers to these problems.

IV. SUMMARY AND CONCLUSIONS

We formulated an excluded-volume HG model and used it to analyze the variations of multiplicity of various particles with respect to the center-of-mass energy $\sqrt{s_{NN}}$ from SIS to RHIC energies. We have also used the present model [11,12] to explain the variations of some particle ratios again with center-of-mass energy and compared our results with the experimental data. A good agreement between our present model results and experimental data supports the claim that thermal model gives a satisfactory description of the data.

In the past we have witnessed the success of ideal gas model in explaining the data, but we know that a correct description of hot, dense hadron gas can be given by a model where hard-core repulsive interactions are incorporated in thermodynamically consistent way. Moreover, at GSI SIS and Brookhaven National Laboratory AGS energies, the freeze-out parameters involve a much larger values of baryon chemical potentials and the predictions of all the excluded-volume models are quite different from those obtained in the ideal gas models. We have already shown the usefulness of the present model in explaining various properties of hot, dense hadron gas [11,12]. The analysis presented here lends further support to our claim that the excluded-volume model obtained by us properly explain the multiplicities and particle ratios of various particles after chemical freeze-out. In conclusion, our model provides a proper and realistic EOS for a hot, dense hadron gas and it can successfully be used at extreme values of the temperatures and/or densities.

ACKNOWLEDGMENTS

One of the authors (M. Mishra) acknowledges the financial support from Council of Scientific and Industrial Research (CSIR), New Delhi. C. P. Singh acknowledges financial support in the form of a Department of Science and Technology (DST) project from Government of India.

[1] H. Satz, Rep. Prog. Phys. **63**, 1511 (2000).
[2] C. P. Singh, Phys. Rep. **236**, 147 (1993).
[3] C. P. Singh, Int. J. Mod. Phys. A **7**, 7185 (1992).
[4] J. Rafelski, Phys. Rep. **88**, 331 (1982).
[5] J. Refelski and R. Hegedorn, *Thermodynamics of Quarks and Hadrons*, edited by H. Satz (North-Holland, Amsterdam, 1981).
[6] J. Rafelski, Nucl. Phys. **A418**, 215c (1984).
[7] J. Rafelski and B. Müller, Phys. Rev. Lett. **48**, 1066 (1982).
[8] P. Koch, B. Müller, and J. Rafelski, Phys. Rep. **142**, 167 (1986).
[9] P. Koch, Prog. Part. Nucl. Phys. **26**, 253 (1991).
[10] H. C. Eggers and J. Rafelski, Int. J. Mod. Phys. A **6**, 1067 (1991).
[11] M. Mishra and C. P. Singh, Phys. Rev. C **76**, 024908 (2007).
[12] M. Mishra and C. P. Singh, Phys. Lett. **B651**, 119 (2007).
[13] A. Andronic, P. Braun-Munzinger, and J. Stachel, Nucl. Phys. **A772**, 167 (2006).
[14] J. Cleymans and H. Satz, Z. Phys. C **57**, 135 (1993).
[15] J. Cleymans and K. Redlich, Phys. Rev. Lett. **81**, 5284 (1998).
[16] J. Cleymans, H. Oeschler, and K. Redlich, Phys. Rev. C **59**, 1663 (1999); Phys. Lett. **B485**, 27 (2000).
[17] P. Braun-Munzinger, I. Heppe, and J. Stachel, Phys. Lett. **B465**, 15 (1999).
[18] P. Braun-Munzinger, D. Magestro, K. Redlich, and J. Stachel, Phys. Lett. **B518**, 41 (2001).
[19] D. H. Rischke, M. I. Gorenstein, H. Stöcker, and W. Greiner, Z. Phys. C **51**, 485 (1991).
[20] J. Cleymans, H. Oeschler, K. Redlich, and S. Wheaton, Phys. Rev. C **73**, 034905 (2006).
[21] J. Cleymans and E. Suhonen, Z. Phys. C **37**, 51 (1987).
[22] F. Becattini, Z. Phys. C **69**, 485 (1996); F. Becattini and U. Heinz, Z. Phys. C **76**, 269 (1997).
[23] J. Cleymans, K. Redlich, and E. Suhonen, Z. Phys. C **51**, 137 (1991).
[24] S. Eidelman *et al.* (Particle Data Group), Phys. Lett. **B592**, 1 (2005).
[25] Berndt Müller and Rajgopal Krishna, Eur. Phys. J. C **43**, 15 (2005).
[26] Oana Ristea (BRAHMS Collaboration), Rom. Rep. Phys. **56**, 659 (2004).
[27] Jipa Alexandru (BRAHMS Collaboration), Acta Phys. Hung. A **22**, 121 (2005).
[28] J. Cleymans, H. Oeschler, K. Redlich, and S. Wheaton, J. Phys. G **32**, S165 (2006).

[29] J. Cleymans and K. Redlich, Phys. Rev. C **60**, 054908 (1999).
[30] P. Braun-Muzinger, J. Cleymans, H. Oeschler, and K. Redlich, Nucl. Phys. **A697**, 902 (2002).
[31] J. Cleymans, H. Oeschler, K. Redlich, and S. Wheaton, Phys. Lett. **B615**, 50 (2005).
[32] C. Blume, J. Phys. G **31**, S57 (2005).
[33] C. Blume *et al*. (NA49 Collaboration), J. Phys. G **31**, S685 (2005).
[34] V. Greco, C. M. Ko, and P. Levai, Phys. Rev. Lett. **90**, 202302 (2003); Phys. Rev. C **68**, 034904 (2003).
[35] R. C. Hwa and C. B. Yang, Phys. Rev. C **67**, 064902 (2003).
[36] R. J. Fries, B. Müller, C. Nonaka, and S. A. Bass, Phys. Rev. Lett. **90**, 202303 (2003).
[37] D. Molnar and S. A. Voloshin, Phys. Rev. Lett. **91**, 092301 (2003).
[38] D. Molnar, J. Phys. G **30**, S1239 (2004).
[39] L. W. Chen and C. M. Ko, Phys. Rev. C **73**, 044903 (2006).
[40] J. L. Klay *et al*. (E895 Collaboration), Phys. Rev. C **68**, 054905 (2003).
[41] S. V. Afanasiev *et al*. (NA49 Collaboration), Phys. Rev. C **66**, 054902 (2002).
[42] M. Gazdzicki *et al*. (NA49 Collaboration), J. Phys. G: Nucl. Part. Phys. **30**, S701 (2004).
[43] I. G. Bearden *et al*. (BRAHMS Collaboration), Phys. Rev. Lett. **94**, 162301 (2005).
[44] T. Anticic *et al*. (NA49 Collaboration), Phys. Rev. Lett. **93**, 022302 (2004).
[45] A. Richard *et al*. (NA49 Collaboration), J. Phys. G: Nucl. Part. Phys. **31**, S115 (2005) (these proceedings).
[46] S. V. Afanasiev *et al*. (NA49 Collaboration), Phys. Lett. **B491**, 59 (2000).
[47] C. Meurer *et al*. (NA49 Collaboration), J. Phys. G: Nucl. Part. Phys. **30**, S1325 (2004).
[48] S. V. Afanasiev *et al*. (NA49 Collaboration), Phys. Lett. **B538**, 275 (2002).
[49] L. Ahle *et al*. (E802 Collaboration), Phys. Rev. C **57**, 466 (1998).
[50] L. Ahle *et al*. (E866 and E917 Collaboration), Phys. Lett. **B476**, 1 (2000).
[51] L. Ahle *et al*. (E866 and E917 Collaboration), Phys. Lett. **B490**, 53 (2000).
[52] L. Ahle *et al*. (E802 Collaboration), Phys. Rev. C **58**, 3523 (1998).
[53] C. Pinkenburg *et al*. (E895 Collaboration), Nucl. Phys. **A698**, 495c (2002).
[54] S. Albergo *et al*. (E896 Collaboration), Phys. Rev. Lett. **88**, 062301 (2002).
[55] F. Becattini, J. Cleymans, A. Keranen, E. Suhonen, and K. Redlich, Phys. Rev. C **64**, 024901 (2001).
[56] P. Chung *et al*. (E895 Collaboration), Phys. Rev. Lett. **91**, 202301 (2003).